

An Embeddable Implicit IUVD Representation for Part-based 3D Human Surface Reconstruction

Baoxing Li, Yong Deng, Yehui Yang, Xu Zhao*, *Member, IEEE*
Department of Automation, Shanghai Jiao Tong University

Abstract—To reconstruct a 3D human surface from a single image, it is important to consider human pose, shape and clothing details simultaneously. In recent years, a combination of parametric body models (such as SMPL) that capture body pose and shape prior, and neural implicit functions that learn flexible clothing details, has been used to integrate the advantages of both approaches. However, the combined representation introduces additional computation, e.g. signed distance calculation, in 3D body feature extraction, which exacerbates the redundancy of the implicit query-and-infer process and fails to preserve the underlying body shape prior. To address these issues, we propose a novel *IUVD-Feedback* representation, which consists of an *IUVD occupancy function* and a *feedback query algorithm*. With this representation, the time-consuming signed distance calculation is replaced by a simple linear transformation in the *IUVD space*, leveraging the SMPL UV maps. Additionally, the redundant query points in the query-and-infer process are reduced through a feedback mechanism. This leads to more reasonable 3D body features and more effective query points, successfully preserving the parametric body prior. Moreover, the *IUVD-Feedback* representation can be embedded into any existing implicit human reconstruction pipelines without modifying the trained neural networks. Experiments on THuman2.0 dataset demonstrate that the proposed *IUVD-Feedback* representation improves result robustness and achieves three times faster acceleration in the query-and-infer process. Furthermore, this representation has the potential to be used in generative applications by leveraging its inherited semantic information from the parametric body model.

Index Terms—3D Human Surface Reconstruction, Implicit Representation, UV Map, Human Body Prior, Acceleration

I. INTRODUCTION

Reconstructing 3D human surface from color images is useful in many applications as mixed reality, film making, virtual try-on and so forth. To date it is still an open problem due to the myriad varieties in human pose, shape and clothing details. To model these varieties, an appropriate 3D human representation is critical. The *parametric body models* [1]–[4], composed by deformable triangle meshes and learnable parameters, are convenient to represent human pose and shape, but lack clothing details. The *neural implicit functions* [5]–[8] can reconstruct clothed humans by indicating whether a space point is inside the human surface [5] or by inferring the signed distance between a space point and the human surface [6], which is called the *query-and-infer* process. The implicit functions perform well in learning the geometric details of human surface but struggle to keep the body prior.

To combine the merits of parametric body models and neural implicit functions, several approaches [9]–[11] have

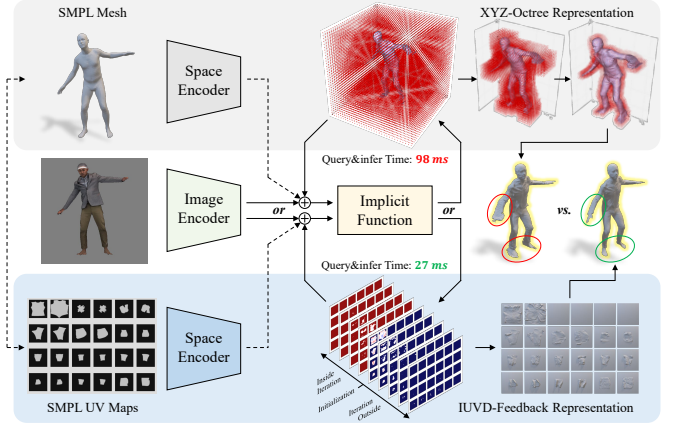


Fig. 1. Comparing the pipelines of implicit human surface reconstruction in the traditional XYZ space and in the proposed IUVD space, there are three advantages of the proposed IUVD-Feedback representation: 1) It accelerates the query&infer and visualization steps, by replacing the redundant SDF calculation and reducing the complexity of marching cubes respectively. 2) It preserves more robust topology of human surface, thus preventing non-human shapes. 3) It produces semantic-aware results, which enables part-based surface editing. Note that the encoders and implicit function modules are replaceable and the space encoders are optional in the pipeline.

been proposed. Their core ideas can be summarized as a *space encoder*, as shown in Fig. 1, that takes an estimated parametric body model, e.g. SMPL [2], as input, and outputs a vector of body features for each space point, as an complement of the image-based features. The combined representations have improved the accuracy of reconstruction results, however, they also introduce additional computation, which may exacerbate the redundancy of the implicit query-and-infer process and reduce the completeness of the underlying body shape prior.

In fact, the problems of the combined representation are caused by two more fundamental problems. One is the compatibility between parametric body models and neural implicit functions, the other is the redundancy of neural implicit functions. **1) Compatibility problem.** It is not trivial to encode the dynamic parametric body mesh into an implicit function because of the gap between the explicit and implicit representations. Taking [11] as an example, it is time-consuming to determine the *signed distance field* (SDF) between the parametric body mesh and space points. This problem has been attacked by replacing the explicit parametric mesh with neural implicit representations [12]–[14]. But these models are unable to reconstruct clothed humans. **2) Redundancy problem.** The implicit query-and-infer process requires massive computation

* Xu Zhao is the corresponding author.

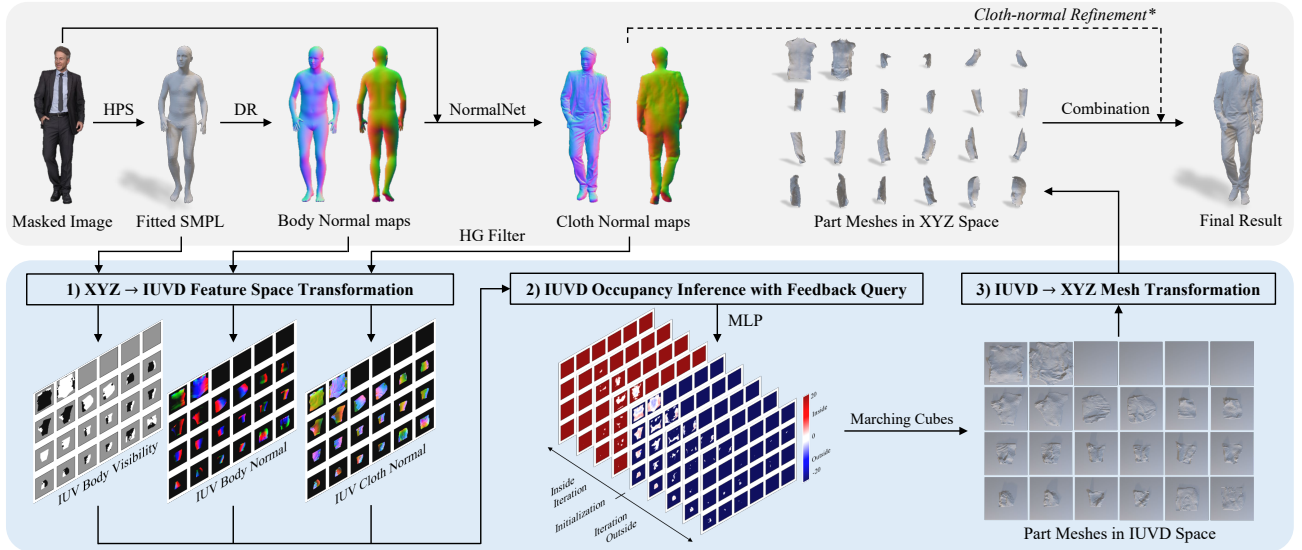


Fig. 2. Overview of 3D human surface reconstruction [11] with the proposed IUVD-Feedback representation. Given a masked color image, we first obtain the SMPL mesh, body normal maps and cloth normal maps where HPS denotes *Human Pose and Shape estimation* and DR denotes *Differentiable Rendering*. Then the implicit 3D human surface reconstruction process is restructured and accelerated in IUVD space (Sec. III) by three steps: 1) XYZ to IUVD feature space transformation (Sec. IV-A), 2) IUVD occupancy inference with feedback query (Sec. IV-B), and 3) IUVD to XYZ mesh transformation (Sec. IV-C). Finally, the part-based meshes are combined and optionally refined in XYZ space as the reconstruction result.

to evaluate the query points far from the human surface, which actually have little contribution to the final result. To reduce this redundancy, Li et al. [15] design an octree-based surface localization algorithm. It successfully eliminates the unnecessary query points, but can not guarantee the robustness of results due to the lack of a human shape prior.

To solve the above two problems simultaneously, we exploit the relationships between parametric body models and neural implicit functions. First, compared to calculating the SDF value given a set of query points and a dynamic body mesh, it is much easier to generate the query points based on the parametric body mesh. Second, the query points near the body mesh are usually more effective for the final visualization, which deserve more attention than those far from the mesh. Inspired by the above observations, we replace the traditional XYZ space with an *IUVD space* based on the unwrapped UV maps [16] of the SMPL model, where $I = 24$ means twenty-four indexed body parts, U and V denote the axes of the 2D texture for part-based SMPL meshes, and D is a clothing deformation axis. In this space, the clothed human is represented by an implicit *IUVD occupancy function*.

In the IUVD space, the compatibility and redundancy problems are solved as following. 1) For the compatibility problem, since the SMPL mesh is unwrapped into UV maps and the part-based meshes are aligned with the IUVD occupancy function, the SDF information is locally decoupled from the pose and shape information. Therefore, the time-consuming SDF calculation can be replaced with a linear transformation, where the query points are generated around the SMPL mesh and the SDF values are simply determined by the D -coordinates. 2) For the redundancy problem, the IUVD space can easily exclude the points far from the human surface, thus eliminating most of the unnecessary query points. To this end, we design a novel *feedback query algorithm*. In this algorithm, the query

points are initialized on the SMPL surface and evaluated iteratively. Taking the previous inference as a feedback, the next batch of query points is generated inside or outside of the SMPL surface along the surface normal directions. By assuming the continuity of the clothed human surface, more than half of the query points can be reduced in this process. By solving the two fundamental problems, the redundancy of the implicit query-and-infer process is largely minimized and the underlying human shape prior is successfully preserved.

The proposed IUVD occupancy function, as well as the feedback query algorithm, collectively called the *IUVD-Feedback* representation, can be embedded into existing implicit 3D human surface reconstruction approaches, such as PIFu [7], PaMIR [9] and ICON [11]. Fig. 1 abstracts the pipelines of these approaches, where the image encoder, space encoder, and implicit function are parameterized by different neural networks. Experiments prove that by replacing the traditional XYZ-Octree representation with the IUVD-Feedback representation, the efficiency and robustness of the reconstruction can be improved. Besides, since the semantic information of SMPL model is fully succeeded by the reconstructed 3D model, it is potential to be used in part-based human surface editing applications.

Fig. 2 shows the usage of the IUVD-Feedback representation in ICON [11]. Given a masked color image of a clothed human, the fitted SMPL model is first estimated by [17] and then rendered to obtain the front and back body normal maps. The input image and body normal maps are fed into a NormalNet [8] to predict the front and back cloth normal maps. Based on these features, the IUVD-Feedback representation is embedded into the implicit reconstruction pipeline by the following three steps. Firstly, the extracted features are transformed from the original XYZ space to IUVD space by UV mapping [18], where a set of *convex assumptions*

is introduced to ensure the equivalence of the feature transformation. Secondly, the proposed feedback query algorithm is used to accelerate the query-and-infer process in IUVD space, where the implicit function does not need to be re-trained. Finally, the body part meshes are separately extracted in IUVD space using marching cubes [19] and then transformed back into XYZ space, which is faster than previous surface localization algorithms. To sum up, the contribution of this paper is three fold.

- 1) A new implicit 3D human representation, IUVD occupancy function, is presented in this paper. This is a general-purpose representation with significant potential to be embedded into existing implicit human surface reconstruction pipelines.
- 2) A novel feedback query algorithm for clothed human surface localization is designed in IUVD space, which reduces more redundancy in implicit human reconstruction than existing octree-based algorithm.
- 3) Experiments show that the proposed IUVD-Feedback representation accelerates the query-and-infer process by three more times than [11], and improves the robustness of results without re-training the neural networks.

II. RELATED WORK

3D human surface reconstruction has been an active research topic for over two decades. We review the approaches related to parametric body models and neural implicit functions, which are the cornerstones of this research.

A. Parametric Human Body Recovery

To represent the 3D human body, statistical body models [1]–[4] are learned from 3D scans and motion capture data [20], thus carrying a robust prior of human pose and shape. These models are parameterized to represent the dynamic human body with an animatable triangle mesh. The parameters of pose and shape can be estimated from color images using optimization-based [21]–[23] or regression-based [24]–[26] methods. Nowadays, the parametric body models have been applied to more complex problems like occluded human estimation [27], [28], temporal human tracking [29], [30], multi-person reconstruction [31], [32], and expressive body recovery [33], [34]. Although the parametric body models can only represent naked bodies, they provide a strong prior of human pose and shape for clothed human surface reconstruction, which is a prerequisite of our method.

B. SMPL-based Human Surface Reconstruction

The SMPL [2] model is one of the most popular parametric body models. However, it is unable to represent clothing details. Alldieck et al. [35] propose to add offsets to the SMPL template mesh for surface deformation, which is called the SMPL+D model. This model has been widely used in clothed human reconstruction [36], [37]. In addition, the SMPL surface can be unwrapped onto images by UV mapping [18]. The visible texture and segmentations can be also mapped into the UV space [38]. Then estimating the offsets of SMPL vertices

is equivalent to estimating a displacement UV map [39], [40]. These surface-based methods have enriched the clothing details of the SMPL model. But the results are restricted to a fixed topology [41] or limited by clothing types [42]. Different from these methods, the proposed representation is designed for both detailed and flexible surface reconstruction.

C. Implicit Human Surface Reconstruction

In addition to the surface-based methods, the 3D human surface can also be reconstructed using volume-based approaches that are not limited by fixed topology. However, explicit voxel-based methods [43], [44] are limited by the large memory cost. In recent years, implicit reconstruction methods have been proposed to solve the problem. Based on learnable implicit functions, such as occupancy functions [7], [8], [45] and signed distance functions [46]–[48] parameterized usually by Multi-Layer Perceptrons (MLPs), the 3D human surface can be reconstructed with unlimited resolution through a memory-efficient query-and-infer process. But their results are sometimes unrealistic or even incomplete due to the lack of human pose and shape priors. Consequently, the parametric body models, e.g. SMPL, have been utilized to extract additional 3D body features [9], [11] as a complementary for the 2D image features. For example, Zheng et al. [9] use a 3D encoder to convert the SMPL model into a 3D feature volume. But the global encoding manner is hard to be generalized to out-of-distribution human poses. Therefore Xiu et al. [11] replace the global body feature with signed distance values as a local body feature, whose results are more robust to pose variations. In this way, the parametric body models successfully preserve the pose and shape priors in implicit human surface reconstruction.

D. Speeding-up Implicit Reconstruction

Although the neural implicit functions are memory-efficient, the query-and-infer process is time-consuming especially when the space resolution is high. Existing researches have proved that redundancy exists in this process. To solve the redundancy, Li et al. [15] design an octree-based coarse-to-fine strategy to reduce the query points far from the reconstructed surface. However, the results could be inaccurate if the segmentation step failed. Feng et al. [49] propose to represent 3D human with a Fourier occupancy field. By discarding the tail terms of the Fourier series, it successfully reduces the redundancy of useless high frequency components. But when the SMPL model is used as an additional input, its running speed is decreased. In contrast, we focus on reducing the redundancy in implicit reconstruction by fully utilizing the parametric body models.

III. IMPLICIT IUVD REPRESENTATION

To represent a 3D clothed human is to simultaneously represent the pose, shape and clothing details of the target person. As the parametric body models, e.g. SMPL [2], have learned the pose and shape information of a naked body, the remaining task is to add displacement on the body mesh, e.g. the SMPL+D [35] model. Differently, we consider to model the clothing deformation in an implicit manner.

We notice that the surface of SMPL model is a 2D compact smooth manifold defined in a 3D Euclidean space, $\Phi \subseteq \mathbb{R}^3$, named as the *XYZ space*. And the SMPL template mesh can be unwrapped onto 24 UV maps corresponding to 24 body parts defined by [16], as shown in Fig. 3 (a), where each pixel, with a non-zero value, of the UV maps corresponds to a 3D point of the SMPL surface. To represent the clothing details, a D-axis is then added orthogonal to the UV-axes, constructing 24 Euclidean IUVD spaces, denoted as $\Psi_i \subseteq \mathbb{R}^3, i = 1, \dots, 24$. The collection of all IUVD spaces is named as the *IUVD space*, $\Psi = \{\Psi_i | i = 1, \dots, I\}$, where $I = 24$ is the number of indexed body parts. Note that the resolution of each IUVD space is theoretically unlimited, thus satisfying the sampling scalability of a general 3D data representation [49]. The shape of the UV plane is formulated by the SMPL UV maps. And the range of D-axis is limited to (D_{min}, D_{max}) , which will be discussed in Sec. IV-A.

To ensure an even density of sampling points in each IUVD space, the SMPL UV maps, denoted as \tilde{M} , are scaled to keep the real proportion of different body parts. Let $\bar{A}_{xyz,i}$ denote the average area of the triangle mesh of the i -th body part in XYZ space, and $\bar{A}_{uv,i}$ denote the average area of the projected triangles on the i -th UV map. The ratio of the average areas is denoted as $r_i = \bar{A}_{xyz,i} / \bar{A}_{uv,i}$. Then the UV coordinates of the projected triangles are updated using Eq. (1). The scaled UV maps are shown in Fig. 3 (b).

$$(u, v)_i := (u, v)_i \cdot \frac{r_i}{\max\{r_i\}}, \quad i = 1, \dots, 24. \quad (1)$$

In IUVD space, the clothed human surface is represented by an implicit *IUVD occupancy function*, denoted as f . Let $\tilde{P}(i, u, v, d) \in \Psi$ denote the query point in IUVD space and $P(x, y, z) \in \Phi$ is the corresponding point in XYZ space. The occupancy value $f(\tilde{P})$ shows the relationship between P and the clothed human surface $S^c \subseteq \Phi$, as defined in Eq. (2).

$$f : \Psi \rightarrow \{0, 1\}. \quad (2)$$

When $f(\tilde{P}) = 0$, the corresponding P is outside the clothed human surface. And when $f(\tilde{P}) = 1$, P is inside the surface. Following [5], this function is approximated with a neural network, f_θ , for binary classification, whose decision boundary implicitly represents the clothed human surface $\tilde{S}^c \subseteq \Psi$.

Meanwhile, the IUVD occupancy function naturally carries the information of parametric body model, as the d coordinate of \tilde{P} indicates the relationship between P and the SMPL mesh of the i -th body part. If $d > 0$, P is outside the SMPL mesh; if $d < 0$, P is inside the SMPL mesh.

IV. IUVD-BASED HUMAN SURFACE RECONSTRUCTION

Given a masked color image and a fitted SMPL model, the 3D human surface can be reconstructed through a learned IUVD occupancy function, f_θ , which is usually parameterized by a Multi-Layer Perceptron (MLP), as shown in Eq. (3).

$$f_\theta(\tilde{P}) = \text{MLP}(\mathcal{F}_{iuvd}(\tilde{P})), \quad \forall \tilde{P} \in \Psi, \quad (3)$$

where $\mathcal{F}_{iuvd}(\tilde{P})$ is the feature vector of \tilde{P} , extracted from the input image and the fitted SMPL model in IUVD space.

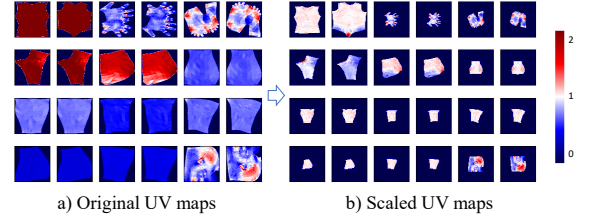


Fig. 3. Scaling the SMPL UV maps for a nearly uniform sampling. The color indicates the proportion of different body parts. The black area is deprecated.

It takes three steps to embed the above IUVD occupancy function into the existing implicit human surface reconstruction pipelines: 1) Converting the feature vectors in XYZ space into IUVD space, i.e. $\mathcal{F}_{xyz}(P) \rightarrow \mathcal{F}_{iuvd}(\tilde{P})$, 2) Inferring the occupancy value $f_\theta(\tilde{P})$ in IUVD space, and 3) Extracting triangle meshes in IUVD space and then transforming them back into XYZ space.

A. XYZ to IUVD Feature Space Transformation

To keep the original performance, we do not change the feature components and the structure of any neural networks. Note that the feature vectors may differ in different implicit functions, but the approach of XYZ-IUVD feature space transformation is similar. Therefore, we take ICON [11] as example in this section, and show the transformation of its local body features from XYZ space to IUVD space. The local body features include the SMPL body normal, the visible cloth normal, and the signed distance based on the closest surface point of the SMPL mesh. The composition and transformation of the local body features in XYZ space and in IUVD space are discussed as follows.

1) *XYZ local body features*. As shown in Fig. 4 (a), for each query point P in XYZ space, the closest point P^b on the estimated SMPL surface $S^b \subseteq \Phi$, and the signed distance $sdf(P, P^b)$ is determined by solving a *point-to-surface* (P2S) optimization problem [50]. This is a time-consuming process. Meanwhile, the projection of P , denoted as x_p is obtained with a weak perspective camera π . The front or back cloth normal of x_p , predicted by a pix2pixHD [51] network (NormalNet), is selected based on the visibility of P^b , denoted as $N_{vis}^c(x_p)$. Finally, the XYZ local body features $\mathcal{F}_{xyz}(P) \in \mathbb{R}^7$ is defined in Eq. (4).

$$\mathcal{F}_{xyz}(P) = [sdf(P, P^b), N^b(P^b), g(N_{vis}^c(x_p))], \quad (4)$$

where $N^b(P^b) \in \mathbb{R}^3$ is the SMPL body normal of P^b , and g is a stacked hourglass [52] network (HGFilter).

2) *IUVD local body features*. Firstly, by UV mapping [18], we build a dense correspondence between the SMPL UV maps and the attributes of SMPL mesh, including vertice position, normal orientation (*IUV body normal*) and visibility information (*IUV body visibility*), as visualized in Fig. 2. Secondly, in IUVD space, we replace the P2S optimization with a simple linear transformation, as shown in Fig. 4 (b), to generate the query points near the SMPL surface S^b . We define the *source point* $\tilde{P}^b(i, u, v) = P^b \in S^b$ corresponding to the query points $P \in \Phi$ along D-axis as shown in Fig. 5

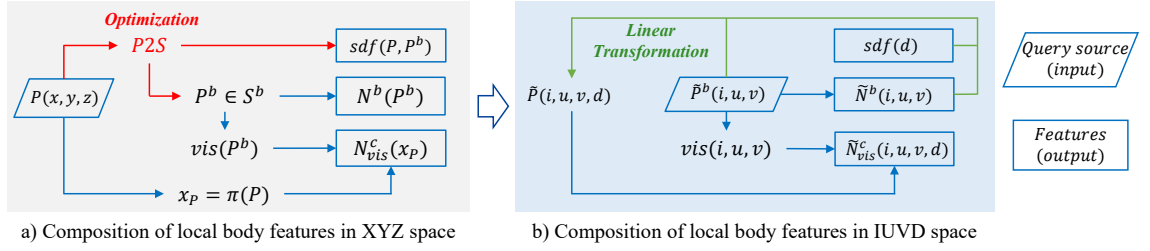


Fig. 4. By changing the source of query points, the local body features in XYZ space are transformed to IUVD space. And the time-consuming P2S optimization (red) is replaced by a simple linear transformation (green) for constructing the IUVD local body features.

(a). Then the XYZ coordinates of P is generated by the linear transformation \mathcal{L} shown in Eq. (5).

$$P(x, y, z) = \mathcal{L}(\tilde{P}) = \tilde{P}^b(i, u, v) + \tilde{N}^b(i, u, v) \cdot sdf(d), \quad (5)$$

where $\tilde{N}^s(i, u, v) = N^b(P^b)$ is the IUVD body normal, $sdf(d) = \alpha \cdot d$, $d \in [D_{min}, D_{max}]$ is a given signed distance function, and α is a scale factor. Finally, based on this linear transformation, the IUVD local body features $\mathcal{F}_{iuvd}(\tilde{P}) \in \mathbb{R}^7$ are derived as Eq. (6).

$$\mathcal{F}_{iuvd}(\tilde{P}) = [sdf(d), \tilde{N}^s(i, u, v), g(\tilde{N}_{vis}^c(i, u, v, d))], \quad (6)$$

where $\tilde{N}_{vis}^c(i, u, v, d) = N_{vis}^c(x_P)$ is the visible IUVD cloth normal shown in Fig. 2.

Note that the correspondence between P and P^b is not always unique, thus the linear transformation \mathcal{L} is noninvertible. Figure 5 (b) shows a non-unique case when the nearby surface is concave. To build a unique dense correspondence from XYZ space to IUVD space, we introduce a set of *convex assumptions* on P and P^b . When these assumptions are satisfied, P is defined as a *valid* query point.

Assumption 1. The neighbourhood of P^b on S^b is convex.

Assumption 2. The query point P is not so far from S^b .

Discussion on Assumption 1. Each part of human body, except the head, hands and feet, can be considered as a rigid object. Following the physical hypothesis that the spherical surface is the most stable shape, the regular surface of each rigid body part should be convex viewed from the outside. As a result, the source point is unique for query points outside the SMPL surface. But for inner points, there may exist multiple source points. So the range of D-axis should be limited to a minimum value, $d > D_{min}$.

Discussion on Assumption 2. When $sdf(d)$ increases, the query point P will be generated far from the SMPL surface. But the precision of P is limited by the precision of $N^b(P^b)$, which is restricted by the triangle mesh. So the range of D-axis should also be limited to a maximum value, $d < D_{max}$. In addition, when different body parts are considered, there will be many alternatives of the source point for a single query point. So the IUVD occupancy function should be visualized in separated UVD spaces for different body parts.

Therefore, the convex assumptions are satisfied when $d \in (D_{min}, D_{max})$ in each UVD space. For simplicity, we assume that all of the query points near the SMPL surface, except hands and feet, are valid. This is proved to be acceptable

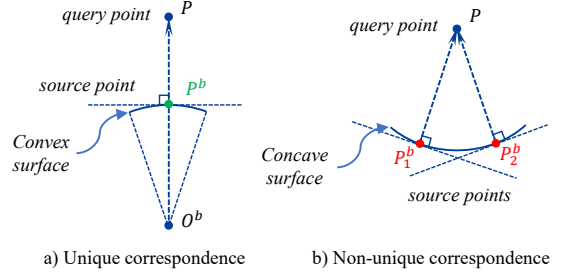


Fig. 5. For a query point P , the corresponding source point P^b is unique when the surface is convex. But there may exist multiple source points, e.g. P_1^b, P_2^b , when the surface is concave.

in our experiments. For each valid query point $\tilde{P} \in \Psi$ and $P \in \Phi$, the IUVD features $\mathcal{F}_{iuvd}(\tilde{P})$ are equal to the XYZ features $\mathcal{F}_{xyz}(P)$ as a result of the convex assumptions. This equivalence property ensures the reconstruction accuracy without retraining the neural networks.

B. IUVD Feedback Query

To localize the 3D human surface from the implicit IUVD occupancy function, different query-and-infer algorithms can be used. In this section, we present three algorithms including full-space query, octree-based query, and a novel feedback query method for accelerating surface localization.

1) *Full-space query & Octree-based query.* A simple idea of the query-and-infer process is to evaluate the IUVD occupancy function in the whole IUVD space, so called the *full-space query*. Based on the voxel grid of each UVD space, all of the voxels \tilde{P} will be visited and the corresponding IUVD local body features are fed into a MLP to predict the occupancy value $f_\theta(\tilde{P}) = \text{MLP}(\mathcal{F}_{iuvd}(\tilde{P}))$. For acceleration, the *octree-based surface localization* algorithm [15] is adopted to subdivide the voxels near the human surface iteratively.

However, experiments show that the above two query methods always fail to generate a reasonable result in IUVD space. The reconstructed surface is always discontinuous especially when the body parts are closely interacted.

2) *Continuity assumptions.* To solve the discontinuity problem, we introduce two assumptions as follows.

Assumption 3. The clothed human surface is a single, continuous layer of mesh between the skin and the clothing.

Assumption 4. The IUVD occupancy function is continuous and locally monotonic along the D-axis.

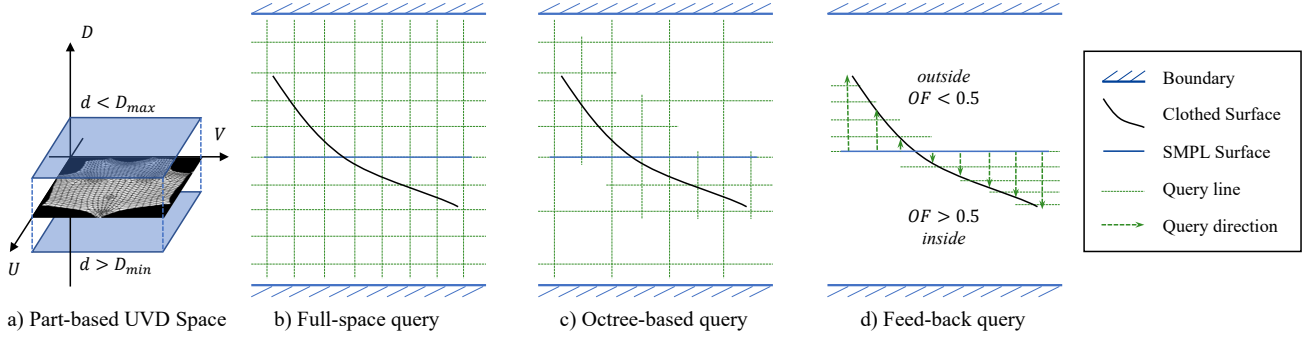


Fig. 6. Illustration of the three query methods in IUVD space, i.e. the collection of part-based UVD spaces. In figure b), c), and d), the blue middle lines denote the SMPL surface. The black curves denote the clothed human surface, where the occupancy value $OF = 0.5$. The intersections of the green dotted lines, which denotes the query lines, and the green dotted lines with arrow, which denotes the query directions, are generated as query points.

The two assumptions ensure the completeness of the results and are easy to satisfy. Under the continuity assumptions, we formulate the implicit surface reconstruction as a locally convex optimization problem, the goal of which is equivalent to finding the optimal d value at each (i, u, v) coordinate.

3) *Feedback query*. Based on the continuity assumptions, we introduce a feedback mechanism into the query-and-infer process, where the IUVD occupancy function is evaluated in a directional and iterative way, as shown in Algorithm 1.

In initialization, the occupancy values of points lying on the SMPL UV maps, $\tilde{P}^b(i, u, v) \in \tilde{M}$, are predicted using Eq. (3). These values generate the *query directions*, $\delta(i, u, v)$, paralleled with the D-axis. Depending on the query directions, the inner/outer points $\tilde{P}_{inner}, \tilde{P}_{outer}$ at (i, u, v) will be set to a maximum/minimum value without inference. This reduces half of the query points.

In each iteration, the d value at (i, u, v) is updated along $\delta(i, u, v)$. The current batch of query points is then generated by Eq. (5). And their occupancy values are inferred using Eq. (3). The iteration at (i, u, v) will stop when the current query point and the previous one are on the opposite side of the clothed human surface, which means the single layer surface is localized. The remaining query points $\tilde{P}_{remains}$ at (i, u, v) will be set to a maximum/minimum value according to their relationship to the surface. Meanwhile, if the D-axis boundary is reached, the iteration will also be terminated.

Note that the complexity of a query algorithm is closely related to the number of query points. In Fig. 6, the query points generated by the three different query methods are denoted as the intersections of query lines and query directions. With similar resolution, the feedback query method produces much less but more reasonable query points, compared to the full-space and octree-based query methods.

C. IUVD to XYZ Mesh Transformation

For visualization, we use marching cubes algorithm [53] separately in each UVD space to extract the triangle meshes of different body parts from the IUVD occupancy function. The part-based meshes are then transformed to XYZ space by applying a linear transformation as Eq. (5) on each vertex. Note that the marching cubes algorithm in IUVD space costs only 8 ms, which is much faster than in XYZ space.

Algorithm 1 IUVD Feedback query

Input: SMPL UV maps \tilde{M} , IUVD local body features $\mathcal{F}_{iuvd}(\tilde{P})$ for each query point $\tilde{P}(i, u, v, d)$

```

1: Initialization:
2: for  $\tilde{P}^b(i, u, v) \in \tilde{M}$  do
3:    $\tilde{P} \leftarrow (i, u, v, 0)$ 
4:    $f_\theta(\tilde{P}) \leftarrow \text{MLP}(\mathcal{F}_{iuvd}(\tilde{P}))$ 
5:   if  $f_\theta(\tilde{P}) > 0.5$  then
6:      $\delta(i, u, v) \leftarrow +1$ 
7:      $f_\theta(\tilde{P}_{inner}) \leftarrow \text{OF}_{max}$ 
8:   else
9:      $\delta(i, u, v) \leftarrow -1$ 
10:     $f_\theta(\tilde{P}_{outer}) \leftarrow \text{OF}_{min}$ 
11:  end if
12: end for
13: Iteration:
14: for  $\tilde{P}^b(i, u, v) \in \tilde{M}$  do
15:    $d \leftarrow 0$ 
16:   repeat
17:      $f_\theta(\tilde{P})^{pre} \leftarrow f_\theta(\tilde{P})$ 
18:      $d \leftarrow d + \delta(i, u, v)$ 
19:      $\tilde{P} \leftarrow (i, u, v, d)$ 
20:      $f_\theta(\tilde{P}) \leftarrow \text{MLP}(\mathcal{F}_{iuvd}(\tilde{P}))$ 
21:   until  $(f_\theta(\tilde{P}) - 0.5) \cdot (f_\theta(\tilde{P})^{pre} - 0.5) < 0$ 
    or  $d > D_{max}$  or  $d < D_{min}$ 
22:    $f_\theta(\tilde{P}_{remains}) \leftarrow \text{sign}(0.5 - f_\theta(\tilde{P})^{pre}) \cdot \text{OF}_{max}$ 
23: end for

```

Output: IUVD occupancy values $\{f_\theta(\tilde{P})\} \in \mathbb{R}^{I \times U \times V \times D}$

To obtain a watertight result, we design a realtime approach that combines offline dilation and online erosion, instead of using the time-consuming Poisson surface reconstruction [54]. In the offline preprocessing, the SMPL UV maps are dilated with a square structuring element and then filled using bilinear extrapolation, which does not effect the online running time. During the online reconstruction, a UV mask-based cropping step is applied to erode the undesired edges of the part-based meshes in IUVD space. With GPU-based parallel acceleration, the additional cropping step costs less than 10 ms.

TABLE I

RUNNING TIME (IN MILLISECONDS) OF ICON [11] WITH DIFFERENT REPRESENTATIONS AT MATCHING RESOLUTIONS. THE *SDF calculation* AND *MLP regression* ARE TWO MAIN STEPS IN THE *query-and-infer* PROCESS. THE *surface extraction* IS TO OBTAIN THE HUMAN MESH, INCLUDING BUT NOT LIMITED TO MARCHING CUBES. NOTE THAT THE PRE-PROCESSING STEPS (E.G. SEGMENTATION [55], HPS ESTIMATION [17]) AND THE CLOTH-NORMAL REFINEMENT ARE NOT INCLUDED IN THIS TABLE SINCE THEY ARE OPTIONAL AND REPLACEABLE IN IMPLICIT RECONSTRUCTION.

Main steps	Representations	XYZ-Full (257^3)	XYZ-Octree [11] (257^3)	IUVD-Full ($24 \times 64^2 \times 21$)	IUVD-Octree ($24 \times 64^2 \times 21$)	IUVD-Feedback (Ours) ($24 \times 64^2 \times 21$)
SDF calculation		3870	52	2	4	2
MLP regression		957	27	26	14	7
Surface extraction		33	25	18	18	18
Query-and-infer		5.1k (5.0k~5.3k)	98 (74~155)	36 (33~38)	28 (25~33)	27 (21~34)
Total (single thread)		5.3k (5.2k~5.5k)	257 (238~310)	183 (178~193)	176 (173~181)	175 (168~189)

TABLE II

COMPARISON ON THE NUMBER OF QUERY POINTS AND THE MARCHING CUBES COMPLEXITY OF ICON [11] WITH DIFFERENT REPRESENTATIONS. THE RESOLUTIONS OF THE XYZ AND IUVD SPACE ARE DENOTED AS $N = 257^3$ AND $M = 24 \times 64^2 \times 21$ CORRESPONDINGLY. NOTE THAT $N > M$.

Representations	XYZ-Full	XYZ-Octree [11]	IUVD-Full	IUVD-Octree	IUVD-Feedback (Ours)
Number of query points	1.6×10^7	1.2×10^5	4.2×10^5	2.2×10^5	5.2×10^4
Marching cubes complexity	$O(N)$	$O(N)$	$O(M)$	$O(M)$	$O(M)$

V. EXPERIMENTS

A. Settings

1) *Dataset and rendering.* The THuman2.0 dataset [56] is used for training and quantitative evaluation. It is a public dataset with 526 high quality textured scans of clothed human and fitted SMPL [2], SMPL-X [3] models. The first 500 scans are used for training. Another 26 scans are used for evaluation.

To obtain the image data, we render the scans of THuman2.0 dataset with a weak perspective camera. Especially, the camera viewpoints consist of 12 horizontal and 3 elevation angles. Other settings follow [11]. It has been proved that the variation of elevation angles helps improve the model accuracy with the same amount of training data.

2) *Training and evaluation.* The experiments take PIFu [7], PaMIR [9], and ICON [11] as baselines. As for PIFu and PaMIR, we use the pretrained models for evaluation. The ICON model, including the NormalNet, HGFilter and MLP mentioned in Sec. IV, is re-trained with the THuman2.0 dataset for 20 epochs on a single NVIDIA GTX 3090 GPU. The training settings follow [11]. Based on these models, we separately evaluate the speed and accuracy improvements brought by the proposed IUVD-Feedback representation.

For speed evaluation, we take ICON as the baseline model and conduct the query-and-infer process using five different representations. Two of them are in XYZ space, including *XYZ-Full* (using full-space query) and *XYZ-Octree* (using octree-based query with three levels). Three of them are in IUVD space, including *IUVD-Full* (using full-space query) and *IUVD-Octree* (using octree-based query with two levels), and *IUVD-Feedback* (using the proposed feedback query). The resolutions of the XYZ space and the IUVD space are set to $257 \times 257 \times 257$ and $24 \times 64 \times 64 \times 21$ to ensure a similar precision. Correspondingly, the scale factor α is set to $1/128$. $D_{max} = 10$, and $D_{min} = -10$. For acceleration, we use the GPU-based marching cubes function of NVIDIA Kaolin

TABLE III

ACCURACY COMPARISON OF PIFu [7], PAMIR [9], AND ICON [11] WITH XYZ-OCTREE OR IUVD-FEEDBACK REPRESENTATIONS ON THUMAN2.0.

Model (Representation)	P2S↓	Chamfer↓	Normal↓
PIFu (XYZ-Octree) [7]	2.824	3.245	0.139
PIFu (IUVD-Feedback)	1.561	1.645	0.116
PaMIR (XYZ-Octree) [9]	1.304	1.941	0.105
PaMIR (IUVD-Feedback)	1.059	1.224	0.080
ICON (XYZ-Octree) [11]	0.832	1.114	0.072
ICON (IUVD-Feedback)	0.925	1.006	0.072
ICON-refine (XYZ-Octree) [11]	0.798	1.082	0.057
ICON-refine (IUVD-Feedback)	0.822	0.906	0.057

TABLE IV

THE AVERAGE RECONSTRUCTION ERROR OF THE SCANS IN THUMAN2.0 DATASET USING IUVD-FULL AND IUVD-FEEDBACK REPRESENTATIONS.

Representation	P2S↓	Chamfer↓	Normal↓
IUVD-Full	0.095	0.075	0.032
IUVD-Feedback	<u>0.159</u>	0.291	<u>0.025</u>
IUVD-Feedback (Poisson)	0.172	<u>0.273</u>	0.023

[57] library to extract surface. For comparison, We report the detailed running time of ICON using the five representations in Table I, where the input image is shown in Fig. 2. The test is repeated for 30 times to avoid random errors. We also compare the number of query points and marching cubes complexity between different representations in Table II.

For accuracy evaluation, we take PIFu, PaMIR, and ICON as the baseline models, and compare the reconstruction accuracy of these models using XYZ-Octree and IUVD-Feedback representations. The evaluation metrics include the point-to-surface distance (*P2S*) and the chamfer distance (*Chamfer*) between the predicted 3D meshes and ground-truth scans, as

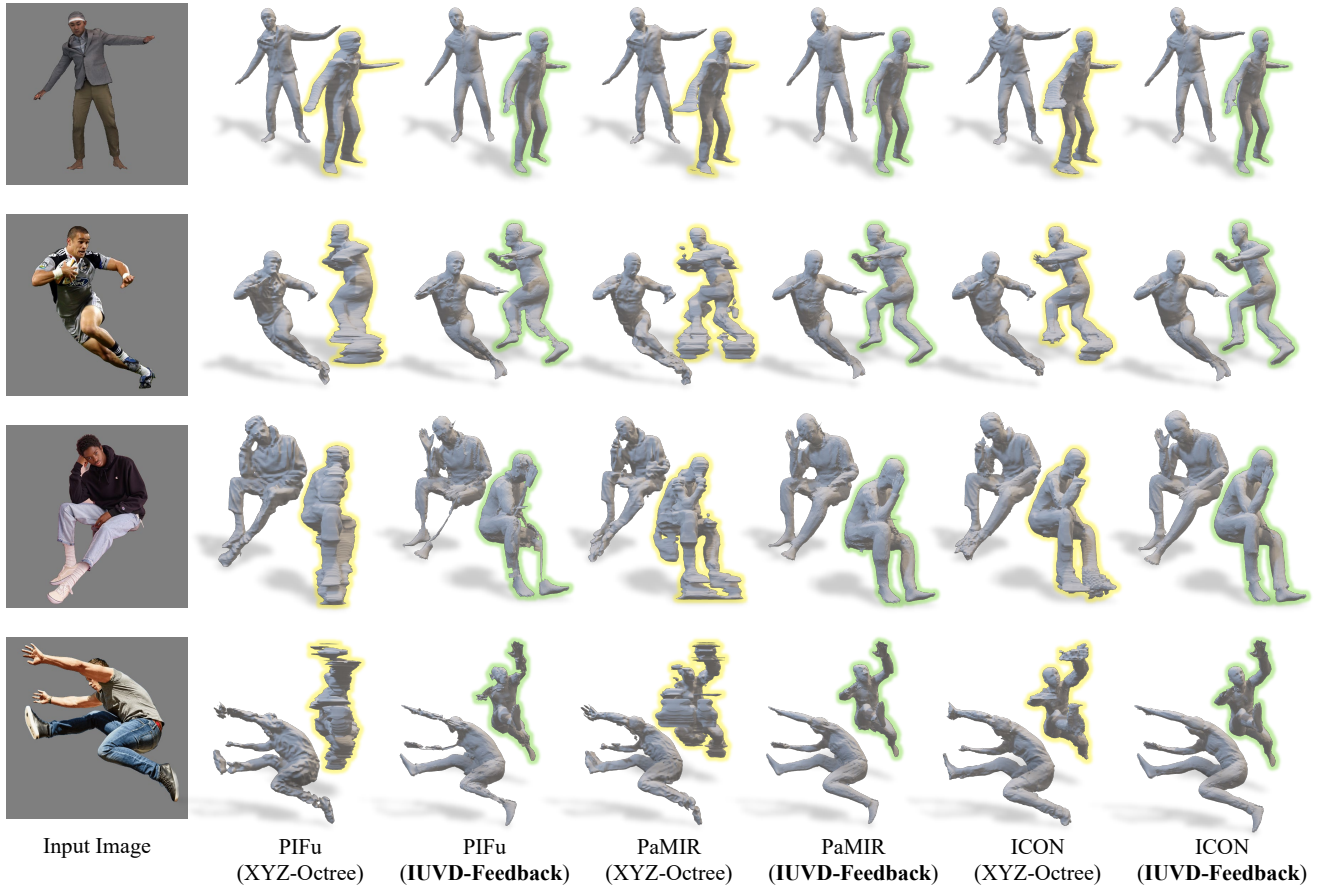


Fig. 7. Qualitative comparison on in-the-wild images with various human poses. Results are obtained by PIFu [7], PaMIR [9] and ICON [11] models with the XYZ-Octree [15] and IUVD-Feedback representations (without cloth-normal refinement). Note that the results highlighted with yellow and green edges are observed from side views, which show the robustness of the proposed IUVD-Feedback representation.

well as the L2 distance between the rendered normal images (*Normal*). When using the IUVD-Feedback representation, the SMPL mesh of hands and feet is preserved to obtain more robust results. The offline cloth-normal refinement step is only used in ICON, denoted as ICON-refine, the implementation of which is the same as [11]. Table III shows the evaluation results on THuman2.0 dataset. Fig. 7 shows the visualization of reconstruction results for in-the-wild images with various human poses. Fig. 8 shows the comparison on clothing details between the XYZ-Octree and IUVD-Feedback representations.

B. Speed Evaluation

Considering the barrel effect, we mainly compare the three most time-consuming steps of ICON, including SDF calculation, MLP regression and surface extraction.

1) *SDF calculation*. As shown in Table I, the SDF calculation is almost the most time-consuming step when using XYZ-Full and XYZ-Octree representations. However, by replacing the P2S optimization with a linear transformation (see Fig. 4) in IUVD space, the time of this step is significantly reduced.

2) *MLP regression*. Note that the MLP regression time is approximately in proportion to the number of query points. Table II shows that the IUVD-Feedback representation reduces the query points by 87.7% than IUVD-Full and by 54.8% than XYZ-Octree. And there is almost no decrease in the accuracy

of ICON, as shown in Table III. Therefore, it proves that the IUVD-Feedback representation successfully reduces the redundancy in the implicit query-and-infer process.

3) *Surface extraction*. To obtain an explicit mesh from the implicit function, the marching cubes algorithm [53] is always required, the time consumption of which is related to the surface geometry and the space resolution [58]. Moreover, in IUVD space, we need additional online erosion and linear transformation for reconstructing a full human mesh (see Sec. IV-C). Totally, the surface extraction time of IUVD-Feedback representation is 72% that of the XYZ-Octree representation. When comparing the time cost of marching cubes, it is shown that the algorithm complexity in IUVD space is 12.2% than that in XYZ space.

4) *Overall comparison*. In summary, the query-and-infer process using IUVD-Feedback representation is over three times faster than using XYZ-Octree representation, which helps reduce about 32% total running time in average. The results prove that the proposed IUVD-Feedback representation is efficient in 3D clothed human surface reconstruction.

C. Accuracy Evaluation

1) *Quantitative comparison*. Table III shows that the IUVD-Feedback representation improves the accuracy of PIFu and PaMIR in all metrics. This is because that PIFu carries

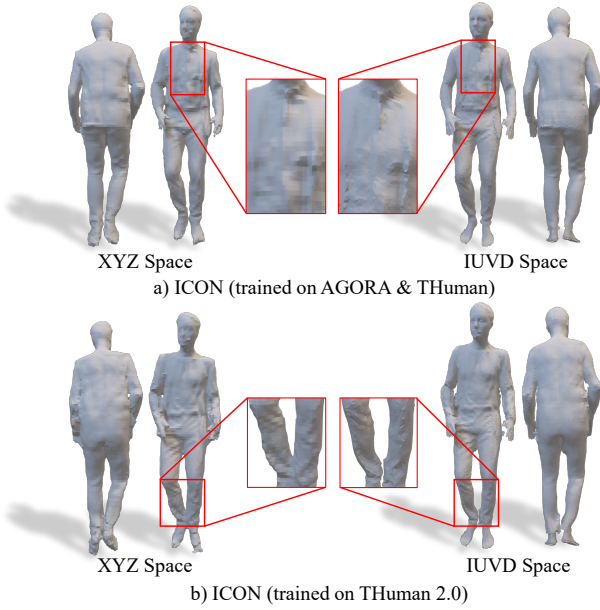


Fig. 8. Comparison of the clothing details reconstructed by ICON in XYZ or IUVD space. The feature equivalence is not effected by the training process.

no prior of SMPL, and PaMIR lacks the out-of-distribution pose prior of SMPL, which can be complemented by the IUVD representation. As for ICON, the results of the two representations have similar accuracy in average, as the SMPL body prior has been utilized by the local body features [11].

2) *Qualitative comparison.* As shown in Fig. 7, the IUVD-Feedback representation improves the robustness of most results, compared to the XYZ-Octree representation. As for PIFu, the IUVD-Feedback makes the side view of the results more recognizable. But since the original results are not properly fitted with the SMPL model, the misaligned parts can not be reconstructed in IUVD space. As for PaMIR, the mis-estimated out-of-body parts are eliminated by the IUVD-Feedback, thus making the results look more cleaner. As for ICON, the IUVD-Feedback produces more reasonable results especially for the limbs of human, where the hands and feet mesh is replaced by the corresponding parts of SMPL mesh. To sum up, the IUVD-Feedback representation makes the reconstruction are more humanlike than the previous results.

3) *Comparison on clothing details.* To prove the equivalence of the local body features in XYZ and IUVD space (see Sec. IV-A), we compare the clothing details reconstructed by ICON using different representations of the two spaces. As shown in Fig. 8, the results reconstructed by XYZ and IUVD representations share the same clothing shape, and the IUVD representation even enhances the geometric details. Meanwhile, a different ICON model is also used for comparison, which is trained on AGORA [59] and THuman [44] datasets by [11]. It proves that the feature equivalence property is not influenced by the training process.

D. Discussion

1) *Volume-based Euclidean space vs. SMPL-based manifold space.* The 3D clothed human surface has been represented

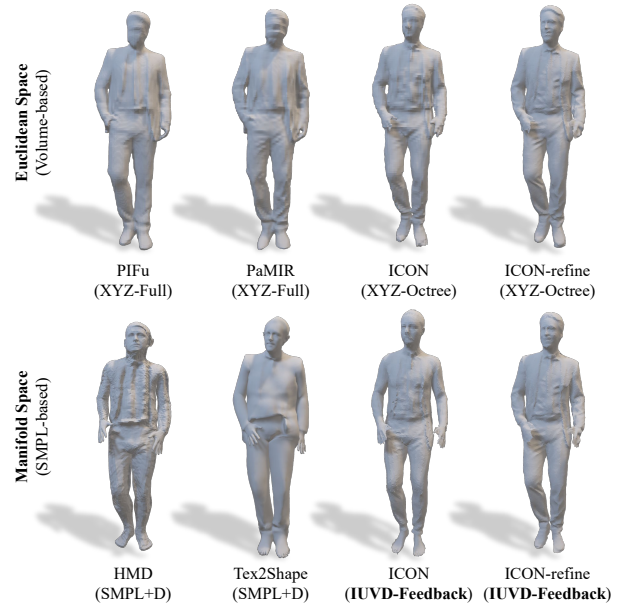


Fig. 9. Comparison of the 3D clothed human surface representations in the volume-based Euclidean (XYZ) space and the SMPL-based manifold space.

either by volume-based representations in an Euclidean space, e.g. PIFu [7] and PaMIR [9], or by SMPL-based surface deformation in a manifold space, e.g. HMD [41] and Tex2Shape [40], as shown in Fig. 9. The proposed IUVD representation, however, *bridges the gap between the two spaces* by bring the volume-based query-and-infer process into the SMPL-based manifold space. It combines the merits of both Volume-based and SMPL-based approaches, including the pixel-aligned features, unlimited resolution and the parametric body prior.

2) *Evaluation of the IUVD representation with ground-truth scans.* To evaluate the upper limit of the proposed IUVD representation, we design an ideal experiment based on THuman2.0 dataset [56]. Firstly, all of the ground-truth scans are transformed into SDF volumes, which are then used to replace the predicted IUVD occupancy values in the query-and-infer process. Secondly, we extract the part-based meshes and combine them in XYZ space as described in Sec. IV-C, thus obtaining the reconstructed human surface meshes. Finally, we calculate the average reconstruction error using *P2S*, *Chamfer* and *Normal* metrics, as shown in Table IV. In this experiment, the resolution of IUVD space is set to $24 \times 128 \times 128 \times 21$ and the scale factor $\alpha = 0.003$. The SMPLX hands and feet mesh is preserved to prevent too much non-unique correspondence problem (see Fig. 5). We also use the Poisson surface reconstruction [54] to smooth the part-based meshes in XYZ space.

It mainly draws two conclusions. Firstly, Table IV shows a fact that the IUVD representation has the potential to achieve higher accuracy if the occupancy value is more accurately predicted. For example, there is nearly no difference between the ground-truth scans in Fig. 10 (a) and the IUVD represented results in Fig. 10 (b) in visualization. Secondly, compared to the full-space query, the feed-back query actually decreases the reconstruction accuracy, due to the continuity assumptions

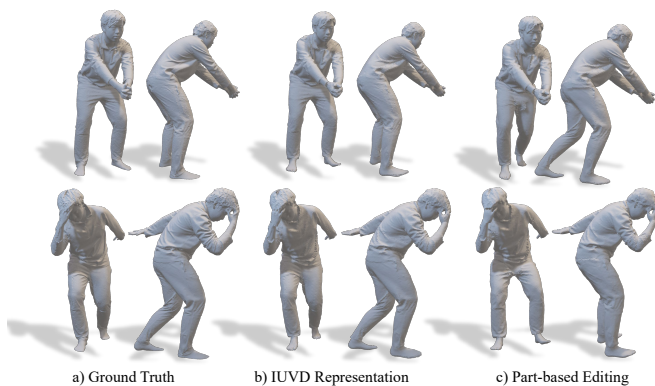


Fig. 10. Reconstruction of the ground-truth scans in THuman2.0 dataset using the IUVD-Feedback representation. The results can be used for part-based surface editing applications.

(see Sec. IV-B), which can be improved in future research.

Based on this experiment, we find that the semantic information of the IUVD representation can be utilized in generative applications. As shown in Fig. 10 (c), by combining the scans with different part indexes, the ground-truth scans can be edited as desired, where the SMPL(X) model is used as an intermediate representation to preserve the body shape.

3) *Limitations of the IUVD representation.* The proposed IUVD-Feedback representation has some limitations. Firstly, the accuracy of HPS strongly affects our approach, which is a common defect in SMPL-based representations. However, thanks to the fast development of the learning-based human mesh recovery methods [60], the impact of this issue has been gradually alleviated. Secondly, there are some hard cases that can not be fully represented by our approach, including loose clothing, braided hair, cuffs, etc., as shown in Fig. 11. Thirdly, when the limbs and body are in contact, the UVD spaces are in risk of overlap, which may lead to confusing results of the part-based meshes. Fourthly, although the transformation between IUVD space and XYZ space is linear, the density mapping between the two space is not strictly uniform. Therefore, it deserves future research for improving this representation.

VI. CONCLUSION

In this paper, we present a new implicit function and a novel feedback query algorithm for 3D human surface reconstruction, named as IUVD-Feedback representation. This representation effectively preserves the human pose and shape prior of the SMPL model, and can be flexibly embedded into existing implicit reconstruction pipelines. Based on the designed feature space transformation and the mesh transformation approaches, the implicit function is evaluated in a SMPL-based IUVD space, thus reducing the redundant query points in the traditional XYZ space. In IUVD space, the redundancy of the query-and-infer process is further reduced by the proposed feedback query algorithm. Experiments show that the robustness of results is improved and the running time of reconstruction is decreased by using the IUVD-Feedback representation. Besides, it is proved that this representation can be applied to generative tasks by exploring the semantic information inherited from the parametric body model.

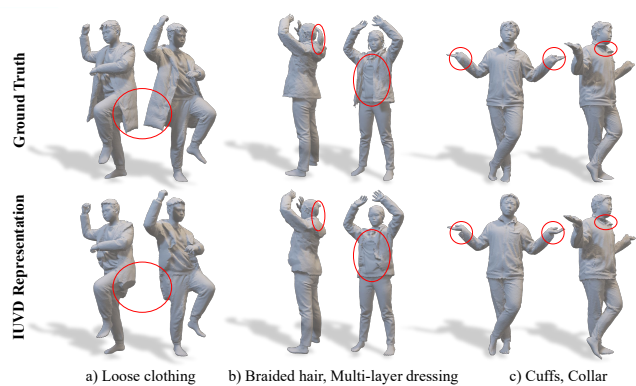


Fig. 11. Hard cases for reconstructing the ground-truth scans of THuman2.0 dataset with the IUVD-Feedback representation.

REFERENCES

- [1] D. Anguelov, P. Srinivasan, D. Koller, S. Thrun, J. Rodgers, and J. Davis, “SCAPE: Shape completion and animation of people,” *ACM Transactions on Graphics*, vol. 24, no. 3, pp. 408–416, 2005.
- [2] M. Loper, N. Mahmood, J. Romero, G. Pons-Moll, and M. J. Black, “SMPL: A skinned multi-person linear model,” *ACM Transactions on Graphics*, vol. 34, no. 6, pp. 248:1–248:16, 2015.
- [3] G. Pavlakos, V. Choutas, N. Ghorbani, T. Bolkart, A. A. Osman, D. Tzionas, and M. J. Black, “Expressive body capture: 3d hands, face, and body from a single image,” in *Proc. IEEE Conference on Computer Vision and Pattern Recognition*, 2019, pp. 10967–10977.
- [4] A. A. A. Osman, T. Bolkart, D. Tzionas, and M. J. Black, “SUPR: A sparse unified part-based human representation,” in *Proc. European Conference on Computer Vision*, 2022, pp. 568–585.
- [5] L. Mescheder, M. Oechsle, M. Niemeyer, S. Nowozin, and A. Geiger, “Occupancy networks: Learning 3d reconstruction in function space,” in *Proc. IEEE Conference on Computer Vision and Pattern Recognition*, 2019, pp. 4455–4465.
- [6] J. J. Park, P. Florence, J. Straub, R. Newcombe, and S. Lovegrove, “DeepSDF: Learning continuous signed distance functions for shape representation,” in *Proc. IEEE Conference on Computer Vision and Pattern Recognition*, 2019, pp. 165–174.
- [7] S. Saito, Z. Huang, R. Natsume, S. Morishima, H. Li, and A. Kanazawa, “PiFu: Pixel-aligned implicit function for high-resolution clothed human digitization,” in *Proc. IEEE International Conference on Computer Vision*, 2019, pp. 2304–2314.
- [8] S. Saito, T. Simon, J. Saragih, and H. Joo, “PiFuHD: Multi-level pixel-aligned implicit function for high-resolution 3d human digitization,” in *Proc. IEEE Conference on Computer Vision and Pattern Recognition*, 2020, pp. 81–90.
- [9] Z. Zheng, T. Yu, Y. Liu, and Q. Dai, “PaMIR: Parametric model-conditioned implicit representation for image-based human reconstruction,” *IEEE Transactions on Pattern Analysis and Machine Intelligence*, vol. 44, no. 6, pp. 3170–3184, 2021.
- [10] Y. Zheng, R. Shao, Y. Zhang, T. Yu, Z. Zheng, Q. Dai, and Y. Liu, “Deep-MultiCap: Performance capture of multiple characters using sparse multiview cameras,” in *Proc. IEEE International Conference on Computer Vision*, 2021, pp. 6239–6249.
- [11] Y. Xiu, J. Yang, D. Tzionas, and M. J. Black, “ICON: Implicit clothed humans obtained from normals,” in *Proc. IEEE Conference on Computer Vision and Pattern Recognition*, 2022, pp. 13 286–13 296.
- [12] B. Deng, J. P. Lewis, T. Jeruzalski, G. Pons-Moll, G. Hinton, M. Norouzi, and A. Tagliasacchi, “NASA neural articulated shape approximation,” in *Proc. European Conference on Computer Vision*, 2020, pp. 612–628.
- [13] T. Alldieck, H. Xu, and C. Sminchisescu, “imGHUM: Implicit generative models of 3d human shape and articulated pose,” in *Proc. IEEE International Conference on Computer Vision*, 2021, pp. 5461–5470.
- [14] M. Mihajlovic, S. Saito, A. Bansal, M. Zollhoefer, and S. Tang, “COAP: Compositional articulated occupancy of people,” in *Proc. IEEE Conference on Computer Vision and Pattern Recognition*, 2022, pp. 13 201–13 210.

- [15] R. Li, Y. Xiu, S. Saito, Z. Huang, K. Olszewski, and H. Li, "Monocular real-time volumetric performance capture," in *Proc. European Conference on Computer Vision*, 2020, pp. 49–67.
- [16] R. A. Güler, N. Neverova, and I. Kokkinos, "DensePose: Dense human pose estimation in the wild," in *Proc. IEEE Conference on Computer Vision and Pattern Recognition*, 2018, pp. 7297–7306.
- [17] H. Zhang, Y. Tian, X. Zhou, W. Ouyang, Y. Liu, L. Wang, and Z. Sun, "PyMAF: 3d human pose and shape regression with pyramidal mesh alignment feedback loop," in *Proc. IEEE International Conference on Computer Vision*, 2021, pp. 11446–11456.
- [18] J. F. Blinn and M. E. Newell, "Texture and reflection in computer generated images," *Communications of the ACM*, vol. 19, no. 10, pp. 542–547, 1976.
- [19] T. S. Newman and H. Yi, "A survey of the marching cubes algorithm," *Computers & Graphics*, vol. 30, no. 5, pp. 854–879, 2006.
- [20] N. Mahmood, N. Ghorbani, N. F. Troje, G. Pons-Moll, and M. Black, "Amass: Archive of motion capture as surface shapes," in *Proc. IEEE International Conference on Computer Vision*, 2019, pp. 5441–5450.
- [21] F. Bogo, A. Kanazawa, C. Lassner, P. Gehler, J. Romero, and M. J. Black, "Keep it smpl: Automatic estimation of 3d human pose and shape from a single image," in *Proc. European Conference on Computer Vision*, 2016, pp. 561–578.
- [22] C. Lassner, J. Romero, M. Kiefel, F. Bogo, M. J. Black, and P. V. Gehler, "Unite the people: Closing the loop between 3d and 2d human representations," in *Proc. IEEE Conference on Computer Vision and Pattern Recognition*, 2017, pp. 4704–4713.
- [23] T. Fan, K. V. Alwala, D. Xiang, W. Xu, T. Murphey, and M. Mukadam, "Revitalizing optimization for 3d human pose and shape estimation: A sparse constrained formulation," in *Proc. IEEE International Conference on Computer Vision*, 2021, pp. 11457–11466.
- [24] A. Kanazawa, M. J. Black, D. W. Jacobs, and J. Malik, "End-to-end recovery of human shape and pose," in *Proc. IEEE Conference on Computer Vision and Pattern Recognition*, 2018, pp. 7122–7131.
- [25] N. Kolotouros, G. Pavlakos, M. J. Black, and K. Daniilidis, "Learning to reconstruct 3d human pose and shape via model-fitting in the loop," in *Proc. IEEE International Conference on Computer Vision*, 2019, pp. 2252–2261.
- [26] M. Kocabas, C.-H. P. Huang, O. Hilliges, and M. J. Black, "PARE: Part attention regressor for 3d human body estimation," in *Proc. IEEE International Conference on Computer Vision*, 2021, pp. 11127–11137.
- [27] R. Khirodkar, S. Tripathi, and K. Kitani, "Occluded human mesh recovery," in *Proc. IEEE Conference on Computer Vision and Pattern Recognition*, 2022, pp. 1715–1725.
- [28] C.-H. Yao, J. Yang, D. Ceylan, Y. Zhou, Y. Zhou, and M.-H. Yang, "Learning visibility for robust dense human body estimation," in *Proc. European Conference on Computer Vision*, 2022, pp. 412–428.
- [29] M. Kocabas, N. Athanasiou, and M. J. Black, "VIBE: Video inference for human body pose and shape estimation," in *Proc. IEEE Conference on Computer Vision and Pattern Recognition*, 2020, pp. 5253–5263.
- [30] H. Choi, G. Moon, J. Y. Chang, and K. M. Lee, "Beyond static features for temporally consistent 3d human pose and shape from a video," in *Proc. IEEE Conference on Computer Vision and Pattern Recognition*, 2021, pp. 1964–1973.
- [31] Y. Sun, Q. Bao, W. Liu, Y. Fu, M. J. Black, and T. Mei, "Monocular, one-stage, regression of multiple 3d people," in *Proc. IEEE International Conference on Computer Vision*, 2021, pp. 11179–11188.
- [32] H. Choi, G. Moon, J. Park, and K. M. Lee, "Learning to estimate robust 3d human mesh from in-the-wild crowded scenes," in *Proc. IEEE Conference on Computer Vision and Pattern Recognition*, 2022, pp. 1475–1484.
- [33] Y. Feng, V. Choutas, T. Bolkart, D. Tzionas, and M. J. Black, "Collaborative regression of expressive bodies using moderation," in *Proc. IEEE International Conference on 3D Vision*, 2021, pp. 792–804.
- [34] H. Zhang, Y. Tian, Y. Zhang, M. Li, L. An, Z. Sun, and Y. Liu, "Pymaf-x: Towards well-aligned full-body model regression from monocular images," *IEEE Transactions on Pattern Analysis and Machine Intelligence*, 2023.
- [35] T. Alldieck, M. Magnor, W. Xu, C. Theobalt, and G. Pons-Moll, "Video based reconstruction of 3d people models," in *Proc. IEEE Conference on Computer Vision and Pattern Recognition*, 2018, pp. 8387–8397.
- [36] G. Moon, H. Nam, T. Shiratori, and K. M. Lee, "3d clothed human reconstruction in the wild," in *Proc. European Conference on Computer Vision*, 2022, pp. 184–200.
- [37] H. Zhao, J. Zhang, Y.-K. Lai, Z. Zheng, Y. Xie, Y. Liu, and K. Li, "High-fidelity human avatars from a single rgb camera," in *Proc. IEEE Conference on Computer Vision and Pattern Recognition*, 2022, pp. 15904–15913.
- [38] T. Alldieck, M. Magnor, W. Xu, C. Theobalt, and G. Pons-Moll, "Detailed human avatars from monocular video," in *Proc. IEEE International Conference on 3D Vision*, 2018, pp. 98–109.
- [39] V. Lazova, E. Insafutdinov, and G. Pons-Moll, "360-degree textures of people in clothing from a single image," in *Proc. IEEE International Conference on 3D Vision*, 2019, pp. 643–653.
- [40] T. Alldieck, G. Pons-Moll, C. Theobalt, and M. Magnor, "Tex2Shape: Detailed full human body geometry from a single image," in *Proc. IEEE International Conference on Computer Vision*, 2019, pp. 2293–2303.
- [41] H. Zhu, X. Zuo, S. Wang, X. Cao, and R. Yang, "Detailed human shape estimation from a single image by hierarchical mesh deformation," in *Proc. IEEE Conference on Computer Vision and Pattern Recognition*, 2019, pp. 4486–4495.
- [42] B. Bhatnagar, G. Tiwari, C. Theobalt, and G. Pons-Moll, "Multi-garment net: Learning to dress 3d people from images," in *Proc. IEEE International Conference on Computer Vision*, 2019, pp. 5419–5429.
- [43] G. Varol, D. Ceylan, B. Russell, J. Yang, E. Yumer, I. Laptev, and C. Schmid, "BodyNet: Volumetric inference of 3d human body shapes," in *Proc. European Conference on Computer Vision*, 2018, pp. 20–38.
- [44] Z. Zheng, T. Yu, Y. Wei, Q. Dai, and Y. Liu, "DeepHuman: 3d human reconstruction from a single image," in *Proc. IEEE International Conference on Computer Vision*, 2019, pp. 7738–7748.
- [45] K. Y. Chan, G. Lin, H. Zhao, and W. Lin, "IntegratedPIFu: Integrated pixel aligned implicit function for single-view human reconstruction," in *Proc. European Conference on Computer Vision*, 2022, pp. 328–344.
- [46] H. Onizuka, Z. Hayirci, D. Thomas, A. Sugimoto, H. Uchiyama, and R.-i. Taniguchi, "TetraTSDF: 3d human reconstruction from a single image with a tetrahedral outer shell," in *Proc. IEEE Conference on Computer Vision and Pattern Recognition*, 2020, pp. 6010–6019.
- [47] B. Jiang, Y. Hong, H. Bao, and J. Zhang, "SelfRecon: Self reconstruction your digital avatar from monocular video," in *Proc. IEEE Conference on Computer Vision and Pattern Recognition*, 2022, pp. 5605–5615.
- [48] T. Alldieck, M. Zanfir, and C. Sminchisescu, "Photorealistic monocular 3d reconstruction of humans wearing clothing," in *Proc. IEEE Conference on Computer Vision and Pattern Recognition*, 2022, pp. 1506–1515.
- [49] Q. Feng, Y. Liu, Y.-K. Lai, J. Yang, and K. Li, "FOF: Learning fourier occupancy field for monocular real-time human reconstruction," in *Advances in Neural Information Processing Systems*, 2022.
- [50] L. M. Zhu, X. M. Zhang, H. Ding, and Y. L. Xiong, "Geometry of signed point-to-surface distance function and its application to surface approximation," *Journal of Computing and Information Science in Engineering*, vol. 10, no. 4, p. 041003, 2010.
- [51] T.-C. Wang, M.-Y. Liu, J.-Y. Zhu, A. Tao, J. Kautz, and B. Catanzaro, "High-resolution image synthesis and semantic manipulation with conditional gans," in *Proc. IEEE Conference on Computer Vision and Pattern Recognition*, 2018, pp. 8798–8807.
- [52] A. Newell, K. Yang, and J. Deng, "Stacked hourglass networks for human pose estimation," in *Proc. European Conference on Computer Vision*, 2016, pp. 483–499.
- [53] W. E. Lorensen and H. E. Cline, "Marching cubes: A high resolution 3d surface construction algorithm," *ACM SIGGRAPH Computer Graphics*, vol. 21, no. 4, pp. 163–169, 1987.
- [54] M. Kazhdan, M. Bolitho, and H. Hoppe, "Poisson surface reconstruction," in *Symposium on Geometry Processing (SGP)*, vol. 7, 2006, p. 0.
- [55] D. Gatis, "Rembg: A tool to remove images background." 2022. [Online]. Available: <https://github.com/danielgatis/rembg>
- [56] T. Yu, Z. Zheng, K. Guo, P. Liu, Q. Dai, and Y. Liu, "Function4D: Real-time human volumetric capture from very sparse consumer rgbd sensors," in *Proc. IEEE Conference on Computer Vision and Pattern Recognition*, 2021, pp. 5742–5752.
- [57] K. M. Jatavallabhula, E. Smith, J.-F. Lafleche, C. F. Tsang, A. Rozantsev, W. Chen, T. Xiang, R. Lebarredian, and S. Fidler, "Kaolin: A pytorch library for accelerating 3d deep learning research," *arXiv preprint arXiv:1911.05063*, 2019.
- [58] X. Huang, X. Chen, T. Tang, and Z. Huang, "Marching cubes algorithm for fast 3d modeling of human face by incremental data fusion," *Mathematical Problems in Engineering*, vol. 2013, 2013.
- [59] P. Patel, C.-H. P. Huang, J. Tesch, D. T. Hoffmann, S. Tripathi, and M. J. Black, "AGORA: Avatars in geography optimized for regression analysis," in *Proc. IEEE Conference on Computer Vision and Pattern Recognition*, 2021, pp. 13463–13473.
- [60] Y. Tian, H. Zhang, Y. Liu, and L. Wang, "Recovering 3d human mesh from monocular images: A survey," *IEEE Transactions on Pattern Analysis and Machine Intelligence*, 2023.